THE JOURNAL OF BIOLOGICAL CHEMISTRY VOL. 289, NO. 12, pp. 8450–8461, March 21, 2014

Central Cavity of Fructose-1,6-bisphosphatase and the Evolution of AMP/Fructose 2,6-bisphosphate Synergism in Eukaryotic Organisms*[S]

Received for publication, January 7, 2014 Published, JBC Papers in Press, January 16, 2014, DOI 10.1074/jbc.M114.548586

Yang Gao, Lu Shen, and Richard B. Honzatko[1]

From the Roy J. Carver Department of Biochemistry, Biophysics and Molecular Biology, Iowa State University, Ames, Iowa 50011

Background: AMP and fructose 2,6-bisphosphate (Fru-2,6-P_2) synergistically inhibit eukaryotic fructose-1,6-bisphosphatase (FBPase). How did this property evolve?
Results: Directed mutations, kinetics, and structure determinations link the central cavity of FBPase to AMP/Fru-2,6-P_2 synergism.
Conclusion: A central cavity in any FBPase implies AMP/Fru-2,6-P_2 and AMP/Fru-6-P synergism.
Significance: AMP/Fru-2,6-P_2 synergism of eukaryotic FBPases probably evolved from AMP/Fru-6-P synergism of an ancestral FBPase.

The effects of AMP and fructose 2,6-bisphosphate (Fru-2,6-P_2) on porcine fructose-1,6-bisphosphatase (*p*FBPase) and *Escherichia coli* FBPase (*e*FBPase) differ in three respects. AMP/Fru-2,6-P_2 synergism in *p*FBPase is absent in *e*FBPase. Fru-2,6-P_2 induces a 13° subunit pair rotation in *p*FBPase but no rotation in *e*FBPase. Hydrophilic side chains in *e*FBPase occupy what otherwise would be a central aqueous cavity observed in *p*FBPase. Explored here is the linkage of AMP/Fru-2,6-P_2 synergism to the central cavity and the evolution of synergism in FBPases. The single mutation $Ser^{45} \rightarrow$ His substantially fills the central cavity of *p*FBPase, and the triple mutation $Ser^{45} \rightarrow$ His, $Thr^{46} \rightarrow$ Arg, and $Leu^{186} \rightarrow$ Tyr replaces porcine with *E. coli* type side chains. Both single and triple mutations significantly reduce synergism while retaining other wild-type kinetic properties. Similar to the effect of Fru-2,6-P_2 on *e*FBPase, the triple mutant of *p*FBPase with bound Fru-2,6-P_2 exhibits only a 2° subunit pair rotation as opposed to the 13° rotation exhibited by the Fru-2,6-P_2 complex of wild-type *p*FBPase. The side chain at position 45 is small in all available eukaryotic FBPases but large and hydrophilic in bacterial FBPases, similar to *e*FBPase. Sequence information indicates the likelihood of synergism in the FBPase from *Leptospira interrogans* (*l*FBPase), and indeed recombinant *l*FBPase exhibits AMP/Fru-2,6-P_2 synergism. Unexpectedly, however, AMP also enhances Fru-6-P binding to *l*FBPase. Taken together, these observations suggest the evolution of AMP/Fru-2,6-P_2 synergism in eukaryotic FBPases from an ancestral FBPase having a central aqueous cavity and exhibiting synergistic feedback inhibition by AMP and Fru-6-P.

Fructose-1,6-bisphosphatase (D-fructose-1,6-bisphosphate 1-phosphohydrolase; EC 3.1.3; FBPase)[2] catalyzes the penultimate step in gluconeogenesis, hydrolyzing fructose 1,6-bisphosphate (Fru-1,6-P_2) to fructose 6-phosphate (Fru-6-P) and phosphate (P_i) (1, 2). Fructose-6-phosphate-1-kinase (PFK-1) in glycolysis opposes the action of FBPase by the ATP-dependent phosphorylation of Fru-6-P (3). The coordinated regulation of FBPase and PFK-1 limits futile cycling *in vivo*. In mammals and presumably other eukaryotes, fructose 2,6-bisphosphate (Fru-2,6-P_2) and AMP inhibit FBPase while activating PFK-1 (3–10). *In vivo* AMP concentrations are nearly constant due to the action of adenylate kinase (11), whereas the level of Fru-2,6-P_2 varies in response to changing nutritional states (10). AMP/Fru-2,6-P_2 synergism in the inhibition of eukaryotic FBPases (5, 6, 12, 13), however, lowers the apparent K_i of AMP as concentrations of Fru-2,6-P_2 increase, making both AMP and Fru-2,6-P_2 dynamic physiological regulators.

Porcine liver FBPase (*p*FBPase) is a model for eukaryotic FBPases (14). Four identical subunits (molecular mass of 37 kDa) form an approximate square-planar arrangement with D2 symmetry. AMP, which binds 28 Å away from the active site (15, 16), is a non-competitive inhibitor with respect to Fru-1,6-P_2 but a competitive inhibitor with respect to catalytically essential divalent cations (Mg^{2+}, Mn^{2+}, or Zn^{2+}) (17, 18). Binding of AMP induces a conformational transition from active R-state to inactive T-state (16, 19). The R- and T-states differ principally by a 15° rotation of the upper relative to the lower subunit pairs of the tetramer and by the displacement of loop 50–72 from an active site-engaged conformation to a disengaged conformation (16). At least two AMP molecules are required for the R- to T-state transition (20). The dimer-dimer interface is the origin of AMP cooperativity (20). Mutations that disrupt interactions between subunit pairs eliminate the coopera-

* This work was supported, in whole or in part, by National Institutes of Health Grant NS 10546.

The atomic coordinates and structure factors (codes 4GWS and 4GWU) have been deposited in the Protein Data Bank (http://wwpdb.org/).

[S] This article contains supplemental Fig. S1.

[1] To whom correspondence should be addressed: Iowa State University, 4206 Mol. Biol. Bldg., Ames, IA 50011. Fax: 515-294-0453; E-mail: honzatko@iastate.edu.

[2] The abbreviations used are: FBPase, fructose-1,6-bisphosphatase; *p*FBPase, porcine liver FBPase; *e*FBPase, *Escherichia coli* FBPase; *l*FBPase, *Leptospira interrogans* FBPase; Fru-1,6-P_2, fructose 1,6-bisphosphate; Fru-2,6-P_2, fructose 2,6-bisphosphate; Fru-6-P, fructose 6-phosphate; PFK-1, fructose-6-phosphate-1-kinase; Glc-6-P, glucose 6-phosphate; PDB, Protein Data Bank.

tive binding of AMP (21, 22). Two AMP-bound intermediate states (I_R-state and I_T-state) have been identified, both of which have engaged loop 50–72 and subunit pair rotations of 3 and 12°, respectively (23, 24). The I_R- and I_T-states exist in AMP complexes because mutations Ala^{54} → Leu and Ile^{10} → Asp, respectively, destabilize the disengaged conformation of loop 50–72.

Fru-2,6-P_2 is a competitive inhibitor with respect to Fru-1,6-P_2 (5, 6). Chemical modification, NMR, mutagenesis, and crystallographic studies consistently indicate Fru-2,6-P_2 binding to the active site (14, 25–28). In the presence of Fru-2,6-P_2, the K_i for AMP falls 10-fold (AMP/Fru-2,6-P_2 synergism) (5, 6, 29). Hines *et al.* (14) suggest that AMP/Fru-2,6-P_2 synergism arises from a similar end state induced independently by AMP and Fru-2,6-P_2, and indeed, Fru-2,6-P_2 and AMP cause comparable subunit pair rotations in *p*FBPase. Moreover, the crystallographic work is in harmony with similar UV spectra of FBPase in complexes with Fru-2,6-P_2 and AMP (14, 29).

Escherichia coli FBPase (*e*FBPase) has 41% sequence identity with *p*FBPase but a fundamentally different mechanism of regulation (30–32). *e*FBPase is subject to feed-forward activation by phosphoenolpyruvate, the binding of which favors an active tetramer over an inactive or less active dimer (30–31). AMP and glucose 6-phosphate (Glc-6-P) are synergistic inhibitors that together drive the enzyme to a T-like state (32). Fru-2,6-P_2, although not present in *E. coli*, is a potent inhibitor of *e*FBPase (14). Unlike *p*FBPase, Fru-2,6-P_2/AMP synergism is absent in the kinetics of *e*FBPase, and, consistent with the hypothesis of Hines *et al.* (14), *e*FBPase remains in the R-state in the presence of Fru-2,6-P_2.

The foregoing begs the following question. If subunit pair rotation in response to Fru-2,6-P_2 is necessary for synergism, then why do subunit pairs rotate in *p*FBPase and not in *e*FBPase? A large water-filled cavity is present at the center of the *p*FBPase tetramer. In *e*FBPase, however, hydrophilic side chains fill the corresponding region. Shown here by directed mutations, kinetics, and structure determinations, the central cavity of *p*FBPase enables the subunit pair rotation of the tetramer in response to Fru-2,6-P_2. Moreover, sequence information implies the existence of bacterial FBPases that probably exhibit AMP/Fru-2,6-P_2 synergism, even in organisms unlikely to produce Fru-2,6-P_2. The FBPase from one such organism, *Leptospira interrogans*, exhibits not only AMP/Fru-2,6-P_2 synergism but also the AMP-enhanced binding of Fru-6-P. Fru-2,6-P_2 as a dynamic regulator of FBPase in eukaryotic systems probably evolved then from a primordial FBPase subject to synergistic feedback inhibition by AMP and Fru-6-P.

EXPERIMENTAL PROCEDURES

Materials—Fru-1,6-P_2, $NADP^+$ and AMP came from Sigma. Fru-2,6-P_2 was prepared by published protocols (33). Glucose-6-phosphate dehydrogenase and phosphoglucose isomerase were purchased from Roche Applied Sciences. The FBPase-deficient *E. coli* strain DF 657 was from the Genetic Stock Center at Yale University. Other chemicals were of reagent grade or equivalent.

Directed Mutations of pFBPase—Mutations were accomplished by specific base changes utilizing the Transformer™ site-directed mutagenesis kit (Clontech). The mutagenic primers were as follows: Ser^{45} → His, 5′-CAAGGCCATC**CA**CACCGCAGTC-3′; Thr^{46} → Arg, 5′-CAAGGCCATCTCC**CG**CGCAGTCCGCAAG-3′; Leu^{186} → Tyr, TGCTTCATG**TAT**GACCCGGCC ATC; Ser^{45} → His/Thr^{46} → Arg, 5′-CAAGGCCATC**CA**C**CG**CGCAGTCCGCAAG-3′ (codons for point mutations are underlined and in boldface type). Ser^{45} → His/Thr^{46} → Arg/Leu^{186} → Tyr *p*FBPase (Cav$^-$ *p*FBPase) came from sequential rounds of mutation using the latter pair of mutagenic primers. Constructs were confirmed by sequencing the promoter region and the entire open reading frame. The Iowa State University sequencing facility provided DNA sequences using the fluorescent dye-dideoxy terminator method.

Expression and Purification of Wild-type and Mutant pFBPases—E. coli strain DF 657 was used for expression of *p*FBPases. The cell culture of *E. coli* DF657, transformed with plasmid, grew to A_{600} of 1.0, at which time transcription was induced by the addition of isopropyl-β-D-thiogalactopyranoside (final concentration 1 mM). The culture was maintained (with shaking, 37 °C) for an additional 16 h before harvesting. The supernatant solution of a cell-free extract was loaded onto a Cibracon Blue-Sepharose column previously equilibrated with 20 mM Tris-HCl, pH 7.5, and 5 mM $MgCl_2$. The column was washed with 20 mM Tris-HCl, pH 7.5. Enzyme was eluted with 5 mM AMP and 20 mM Tris-HCl, pH 7.5. The pH of eluted protein solution was adjusted to 8.5 before loading onto a DEAE-Sepharose column equilibrated with 20 mM Tris-HCl, pH 8.3. Purified enzyme was eluted with a NaCl gradient (0–0.5 M) in 10 mM Tris-HCl, pH 8.3, and then dialyzed extensively against 50 mM Hepes, pH 7.4, for kinetic investigations and for crystallization experiments. Purity and protein concentrations of FBPase preparations were confirmed by SDS-PAGE (34) and by the Bradford assay (35), respectively.

Cloning, Expression, and Purification of lFBPase—The gene for *l*FBPase (UniProt ID Q8F421) was synthesized and cloned into a pET24b plasmid from Genscript. The integrity of the construct was confirmed by sequencing the promoter region and the entire open reading frame as above for mutant constructs of *p*FBPase. Expression of *l*FBPase followed the procedure outlined above for *p*FBPase. The supernatant component of the cell-free extract was subject to ammonium sulfate fractionation. The 30–50% ammonium sulfate fraction was collected and dialyzed in 20 mM Tris, pH 8.0, before loading onto a DEAE-Sepharose column. Purified enzyme was eluted with a NaCl gradient (0–0.5 M) in 20 mM Tris-HCl, pH 8.0. Enzyme was dialyzed extensively against 50 mM Hepes, pH 7.4, for kinetics studies. Purity and protein concentrations of *l*FBPase preparations were confirmed by SDS-PAGE (34) and by Bradford assay (35), respectively.

Kinetics—Phosphoglucose isomerase and glucose-6-phosphate dehydrogenase were used as coupling enzymes in assays for FBPase (1). For specific activity measurements, reduction of NADP to NADPH was monitored by absorbance at 340 nm. Other assays used the same coupling enzymes but monitored the formation of NADPH by its fluorescence emission at 470 nm using an excitation wavelength of 340 nm. Assays were performed at 22 °C in 50 mM Hepes, pH 7.5. Assay solutions for wild-type and mutant *p*FBPases contained EDTA and KCl at concentrations of 10 μM and 150 mM, respectively, whereas KCl was absent in the assay solution for *l*FBPase. Data for AMP inhibition with respect to Mg^{2+} and Fru-

2,6-P_2 inhibition with respect to Fru-1,6-P_2 were fit to several models using Grafit (36), with best fits of data to models reported here.

Tryptophan Fluorescence—Fluorescence measurements were made at room temperature using a 1-cm^2 quartz cuvette on an SLM Amico 8000 fluorometer. The excitation wavelength was 295 nm, and emission scans were integrated from 310 to 370 nm. Fluorescence scans (repeat of three scans for each data point) were performed after the additions of small volumes of ligand to 2 ml of a 2 μM *l*FBPase solution. The total volume of added titrant did not exceed 1% of the initial volume. Data fitting was carried out using protocols in the literature (37).

Crystallization of Cav$^-$ pFBPase—The method of hanging drops combined 2 μl of protein solution with 2 μl of precipitant solution. Wells contained 500 μl of the precipitant solution. Crystals of the Fru-2,6-P_2 complex grew from a protein solution (10 mg/ml Cav$^-$ FBPase, 25 mM Hepes, pH 7.4, 5 mM $MgCl_2$, and 5 mM Fru-2,6-P_2) combined with a precipitant solution (100 mM Hepes, pH 7.4, 8% (w/v) polyethylene glycol 3350, 27% (v/v) glycerol, and 5% (v/v) *t*-butyl alcohol). Crystals of the AMP complex grew from a protein solution (10 mg/ml Cav$^-$ FBPase, 25 mM Hepes, pH 7.4, 5 mM $MgCl_2$, and 5 mM AMP) combined with a precipitant solution (100 mM Hepes, pH 7.4, 12% (w/v) polyethylene glycol 3350, 23% (v/v) glycerol, and 5% (v/v) *t*-butyl alcohol). Crystals were of equal dimensions (0.2–0.4 mm), growing in ~3 days at 20 °C, and were transferred directly from droplet to liquid nitrogen as cryoprotectants were included in the conditions of crystallization.

X-ray Data Collection, Structure Determination, and Refinement—Data were collected at Iowa State University from single crystals on a Rigaku R-AXIS IV++ rotating anode/image plate system using CuK_α radiation from an Osmic confocal optics system and a temperature of 110 K. The program d*trek (38) was used in reducing data.

Cav$^-$ FBPase with Fru-2,6-P_2 and AMP are isomorphous to R- and T-state FBPase complexes, respectively. R-state FBPase (PDB code 1CNQ) and T-state FBPase (PDB code 1EYJ) were used as initial models for molecular replacement. The resulting models underwent refinement using CNS (39) with force constants and parameters of stereochemistry from Engh and Huber (40). A cycle of refinement consisted of slow cooling from 1000 to 300 K in steps of 25 K followed by 100 cycles of conjugate gradient minimization and concluded by the refinement of individual thermal parameters. Restraints of 1.5 $Å^2$ on nearest neighbor and next-to-nearest neighbor main chain atoms, 2.0 $Å^2$ on nearest neighbor side chain atoms, and 2.5 $Å^2$ on next-to-nearest neighbor side chain atoms were employed in thermal parameter refinement. Water molecules were added to difference electron density of 2.5σ or better until no significant decrease was evident in the R_{free} value. Water molecules in the final models were within acceptable donor-acceptor distances to each other and/or a polar group of the protein. Stereochemistry of the models was analyzed by use of MolProbity (41).

RESULTS

Rationale for Directed Mutations—Directed mutations have identified residues essential for AMP binding (20, 42), regulation (43–46), cooperativity (21–22, 43), and Fru-2,6-P_2 binding (47); however, no mutation eliminates AMP/Fru-2,6-P_2 synergism while retaining potent AMP and Fru-2,6-P_2 inhibition. Because *e*FBPase shares 41% identity with *p*FBPase but lacks AMP/Fru-2,6-P_2 synergism, some subset of the remaining 59% of residues must be responsible.

An overview of FBPase showing the relationship of ligand binding sites and loop 50–72 to the central cavity appears in Fig. 1. The number of water molecules in the central cavities of *p*FBPases, varying in quaternary state and loop conformation (PDB codes 1CNQ, 1NUY, 1YYZ, 2F3D, 2QVV, 2QVU, 1EYJ, and 1FRP), averages to 31, and that of a similar ensemble of *e*FBPases (PDB codes 2OX3, 2QVR, 2GQ1, and 2Q8M) averages to 14 (supplemental Fig. S1). The difference in water structures of the central cavities of *p*FBPase and *e*FBPase is not solely due to the resolution of crystal structures because cavities with the highest numbers of discrete sites for water molecules in *e*FBPase (2GQ1; 22 water molecules, 1.5 Å resolution) and *p*FBPase (1YYZ; 48 water molecules, 1.9 Å resolution) follow the trend established by the ensemble averages (Fig. 1). Order/disorder transitions of water molecules in the cavity could be a factor in AMP/inhibitor synergism. Only three positions in or near the central cavity differ in residue type between *e*FBPase and *p*FBPase. Ser^{45}, Thr^{46}, and Leu^{186} in the porcine enzyme are His^{37}, Arg^{38}, and Tyr^{180}, respectively, in *e*FBPase (Fig. 1). Side chains of Ser^{45}/His^{37} point into the central cavity, whereas side chains of Thr^{46}/Arg^{38} and Leu^{186}/Tyr^{180} are at the edge. If the central cavity is essential to synergism, then mutations that replace residues of *p*FBPase with those of *e*FBPase should significantly reduce AMP/Fru-2,6-P_2 synergism.

Kinetics of Wild-type and Mutant pFBPases—His^{45}, Arg^{46}, and Cav$^-$ FBPase have substantial activity relative to wild-type enzyme (Table 1). The K_m for substrate for Tyr^{186} *p*FBPase is 2-fold greater than that for wild-type enzyme. Mutations cause only minor changes in the K_a for Mg^{2+}. AMP is a competitive inhibitor with respect to Mg^{2+} for all mutants. Hill coefficients of ~2 indicate positive cooperativity in AMP binding. The K_i of AMP for Arg^{46} *p*FBPase decreases 6-fold, whereas for other mutants, the K_i for AMP inhibition is comparable with that of wild-type enzyme. His^{45}, Arg^{46}, and Cav$^-$ *p*FBPases exhibit residual activity (10–20% of V_{max}) at saturating levels of AMP. This phenomenon has been attributed to active AMP complexes in intermediate quaternary states of the tetramer (24, 45). Fru-2,6-P_2 is a potent inhibitor, competitive with respect to Fru-1,6-P_2 for all FBPases here. In general, cavity mutations have relatively minor effects on activity and ligand binding affinities.

Data in Fig. 2 represent the linear increase in fluorescence with time due to the production of NADPH. In previous work (14), each curve was fit by an empirical relationship with adjustable parameters for maximal and minimum velocities and a Hill coefficient and then replotted as relative velocity *versus* [AMP]. An alternative model-based definition of synergism (Scheme 1) provides an analytical expression valid at all concentrations of Fru-2,6-P_2, including an infinite concentration.

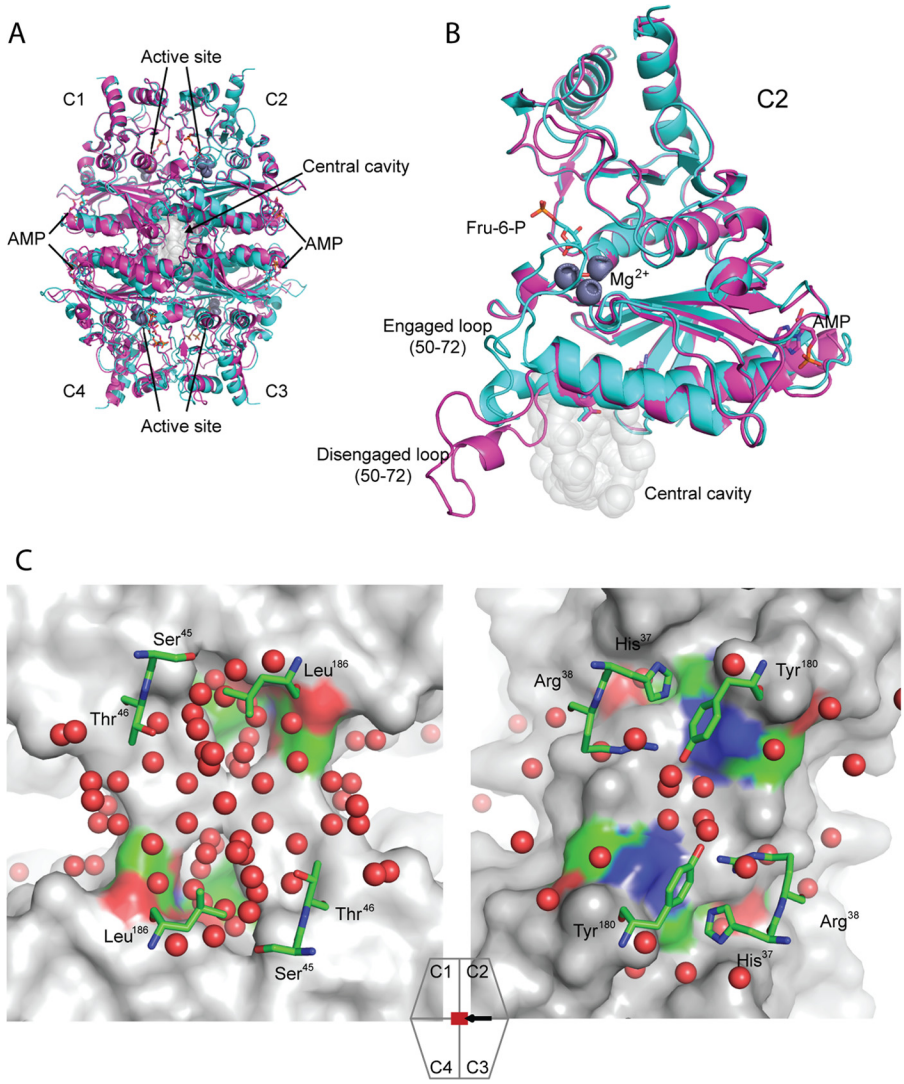

FIGURE 1. **Overview of FBPases.** *A*, alignment of R-state (*cyan*, product complex, PDB code 1CNQ) and T-state (*magenta*, AMP complex, PDB code 1EYJ) *p*FBPases map the locations of AMP binding, active sites, and the central cavity. *B*, an *expanded view* of *A*, showing subunit C2 with loop 50–72 in engaged (*cyan*) and disengaged (*magenta*) conformations. *C*, the central cavity of Leu^{54} *p*FBPase (*left*, I_R-state, AMP complex, 1.9 Å, PDB code 1YYZ) and the central region of *e*FBPase (*right*, ammonium sulfate complex, 1.5 Å, PDB code 2GQ1). Comparable regions exhibit significant differences in hydration levels. The *surface renderings* are of subunits C1 and C4 of the tetramer, with *ball-and-stick models* representing selected residues from subunits C2 and C3 and water molecules (*red spheres*). The *icon* with associated *arrow* indicates the region viewed and viewing direction, respectively. Image generated with PyMOL (57).

TABLE 1

Parameters from the kinetics of wild-type and mutant forms of *p*FBPases and wild type/FBPase

Values in parenthesis are standard deviations in the last significant digit.

	Specific activity[a]	K_m Fru-1,6-P_2[b]	Hill coefficient Mg^{2+}[c]	K_a Mg^{2+}[d]	Hill coefficient AMP[e]	K_i AMP[f]	K_i Fru-2,6-P_2[g]
	$\mu mol\ s^{-1}\ mg^{-1}$	μM		mM		μM^2	μM
WT *p*FBPase	25 (1)	1.47 (7)	1.7 (1)	0.70 (5)	2.2 (1)	0.76 (8)	0.14 (1)
S45H *p*FBPase	11.9 (7)	1.07 (7)	1.6 (1)	1.0 (1)	1.8 (1)	0.35 (5)	0.053 (9)
T46R *p*FBPase	12.3 (9)	0.68 (8)	1.8 (2)	0.93 (9)	2.4 (2)	4.8 (2)	0.27 (5)
L186Y *p*FBPase	21.0 (7)	1.1 (1)	1.6 (1)	0.68 (4)	1.7 (2)	0.58 (9)	0.16 (1)
Cav^- *p*FBPase	15.2 (9)	1.1 (2)	1.8 (1)	0.82 (6)	2.2 (2)	0.56 (4)	0.14 (1)
*l*FBPase	15 (1)	1.0 (1)	0.77 (8)	1.3 (1)	2.2 (2)	0.58 (5)	0.05 (1)

[a] Determined at saturating Fru-1,6-P_2 (20 μM) and saturating Mg^{2+} (5 mM for wild-type *p*FBPase and *l*FBPase and 10 mM for mutant *p*FBPases). Reported values come from five repetitions.

[b] Determined at saturating Mg^{2+} (5 mM for wild-type *p*FBPase and *l*FBPase and 10 mM for mutant *p*FBPases). The concentrations of Fru-1,6-P_2 vary from 0.3 to 20 μM.

[c] Hill coefficient for Mg^{2+} employed 0.2–20 mM Mg^{2+} and saturating Fru-1,6-P_2 (20 μM).

[d] Determined by using concentrations in Mg^{2+} from 0.5 to 5 mM and Fru-1,6-P_2 from 0.5 to 10 μM.

[e] Determined by using concentrations in AMP from 0.1 to 100 μM and saturating Fru-1,6-P_2 (20 μM) and Mg^{2+} (10 mM).

[f] Determined by using concentrations in Mg^{2+} from 0.5 to 5 mM with saturating Fru-1,6-P_2 (20 μM). AMP concentrations range from 0 to 5 μM for wild-type *p*FBPase and *l*FBPase, from 0 to 3 μM for His^{45} *p*FBPase, from 0 to 20 μM for Arg^{46} *p*FBPase, and from 0 to 5 μM for Tyr^{186} and Cav^- *p*FBPases.

[g] Determined by using Mg^{2+} (5 mM for wild-type *p*FBPase and *l*FBPase and 10 mM for mutant *p*FBPases) and Fru-1,6-P_2 concentrations from 0.5 to 10 μM. Concentrations of Fru-2,6-P_2 range from 0 to 1 μM for wild-type *p*FBPase, from 0 to 0.5 μM for His^{45} *p*FBPase and *l*FBPase, from 0 to 1 μM for Arg^{46} *p*FBPase, and from 0 to 1 μM for Tyr^{186} *p*FBPase and Cav^- *p*FBPases.

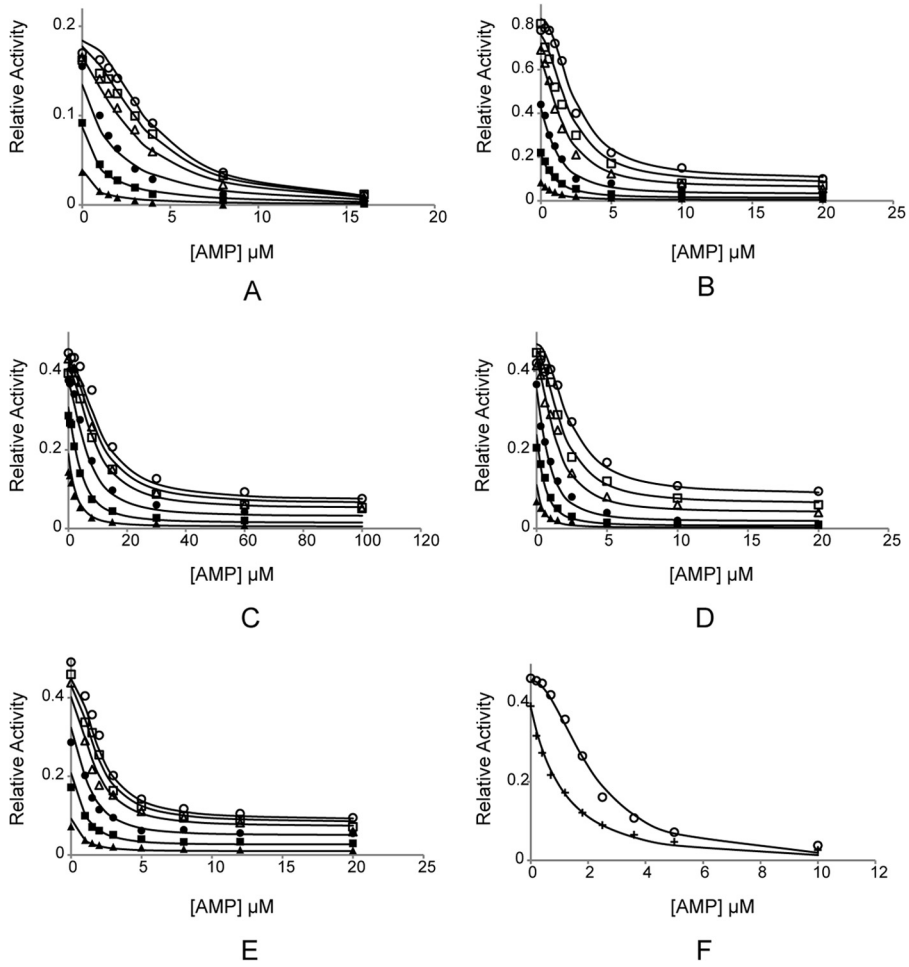

FIGURE 2. **AMP/Fru-2,6-P_2 synergism for wild-type and mutant FBPases.** *A–E*, from assays using wild-type, His[45], Arg[46], Tyr[186], and Cav$^-$ *p*FBPases, respectively. Reaction velocities as a function of AMP concentration are taken at 0 (○), 0.1 (□), 0.3 (△), 1 (●), 3 (■), and 10 μM (▲) Fru-2,6-P_2. *F*, from AMP inhibition assays with wild-type *l*FBPase at 0 (○) and 0.33 μM (+) Fru-2,6-P_2. In all assays, the concentration of Fru-1,6-P_2 is 20 μM, and that of Mg^{2+} is 10 mM.

$$E + 2A = EA_2;\ K_{iaa}$$
$$E + B = EB;\ K_{ib}$$
$$EB + A = EBA;\ K_{iba}$$
$$EBA + A = EBA_2;\ K_{ibaa} = 4K_{iba}$$
$$E + S = ES;\ K_s$$
$$EA_2 + S = ESA_2;\ K_{isaa}$$
$$ES \rightarrow \text{products};\ k_{cat}$$
$$ESA_2 \rightarrow \text{products};\ k'_{cat}$$

SCHEME 1

In Scheme I, substrate *S* binds to FBPase subunits independently (48), resulting in an *ES* complex that contributes to activity (k_{cat}). Two molecules of AMP (represented by *A*) bind with a Hill coefficient of 2 and affect an R- to T-state transition (20). The ESA_2 complexes for some mutant *p*FBPases retain residual activity (k_{cat}' is nonzero). Fru-2,6-P_2 (represented by *B*) and substrate are mutually exclusive in binding to the enzyme (5, 6); however, the binding of AMP and substrate are not mutually exclusive (43). AMP and Fru-2,6-P_2 bind to distinct sites (*EBA* and EBA_2). The Hill coefficient for AMP becomes unity in the presence of Fru-2,6-P_2. Hence, the equilibrium constant (K_{ibaa}) for the binding of *A* to *EBA* equals $4K_{iba}$, as required for the independent binding of ligands to two identical sites.

Equation 1 gives the velocity *v* based on Scheme 1.

$$v = (SV_{max}/K_s)(1 + (k_{cat}'/(k_{cat}K_{issa}))A^2)/(1 + (S/K_s) + (1/K_{iaa} + S/(K_sK_{isaa}))A^2 + B/K_{ib} + BA/(K_{ib}K_{iba}) + BA^2/(4K_{ib}K_{iba}^2)) \quad \text{(Eq. 1)}$$

In fitting Equation 1, V_{max}, $k_{cat}'/(k_{cat}K_{issa})$, $(1/K_{iaa} + S/(K_sK_{isaa}))$, and K_{iba} are adjustable parameters. K_s and K_{ib} are determined by separate experiments for each enzyme (K_m and K_i Fru-2,6-P_2 of Table 1, respectively), and *S* is 20 μM for all determinations. Values for parameters for each FBPase are shown in Table 2 with fits of Equation 1 in Fig. 2.

Rewriting Equation 1 with *A* as the independent variable leads to Equation 2,

$$aA_{0.5}^2 + bA_{0.50} + c = 0 \quad \text{(Eq. 2)}$$

where $a = (v_{0.5})(1/K_{iaa} + S/K_SK_{isaa} + B/4K_{ib}K_{iba}^2) - SV_{max}k'_{cat}/K_SK_{issa}k_{cat}$; $b = (v_{0.5})(B/(K_{ib}K_{iba}))$; $c = (v_{0.5})(1 + S/K_S + B/K_{ib}) - SV_{max}/K_S$; and $v_{0.5}$ is one-half of the sum of the maximum (at $A = 0$) and minimum (at $A = \infty$) velocities for a given concentration of *B*. The quadratic formula provides $A_{0.5}$ at any value of *B* including $B = \infty$ (Table 2). Synergism is defined here

TABLE 2
Fru-2,6-P_2/AMP synergism of FBPases
Values in parentheses are uncertainties in the last significant digit.

	WT *p*FBPase	S45H *p*FBPase	T46R *p*FBPase	L186Y *p*FBPase	Cav^- *p*FBPase	WT *l*FBPase
V_{max} (arbitrary units min^{-1})	0.194 (4)	0.88 (3)	0.434 (8)	0.495 (9)	0.47 (1)	0.48 (1)
$(k'_{cat}/(k_{cat}K_{issa})$ (μM^{-2})	0[a]	0.0018 (4)	0.0006 (1)	0.0017 (2)	0.0024 (3)	0[a]
K_{iba} (μM)	0.51 (4)	0.30 (2)	4.1 (5)	0.28 (3)	0.20 (2)	0.21 (1)
$(1/K_{iaa} + S/(K_sK_{isaa}))$ (μM^{-2})	0.78 (6)	0.85 (6)	1.7 (1)	0.35 (3)	0.72 (4)	0.17 (2)
$A_{0.5}^{B=\infty}$ (μM)	0.42 (4)	0.71 (6)	1.4 (1)	0.29 (3)	0.60 (4)	0.14 (2)
$A_{0.5}^{B=0}$ (μM)	3.9 (3)	2.4 (2)	11 (1)	2.3 (2)	2.0 (2)	2.1 (2)
$A_{0.5}^{B=0}/A_{0.5}^{B=\infty}$	9 (1)	3.4 (9)	8 (1)	8 (2)	3.3 (6)	15 (4)

[a] Value fixed to zero, reflecting full inhibition at saturating concentrations of AMP.

as $A_{0.5}^{B=0}/A_{0.5}^{B=\infty}$. For wild-type, Arg^{46}, and Tyr^{186} *p*FBPases, $A_{0.5}$ decreases significantly as Fru-2,6-P_2 concentration increases. On the other hand, His^{45} and Cav^- *p*FBPases show a two-thirds loss of AMP/Fru-2,6-P_2 synergism (Table 2).

AMP Complex of Cav^- pFBPase (Protein Data Bank Code 4GWS)—Crystals of the AMP complex of Cav^- *p*FBPase (space group $P2_12_12$, a = 60.24 Å, b = 164.29 Å, and c = 79.14 Å) belong to the same space group and lattice as crystals of canonical T-state *p*FBPase. A C1-C2 dimer exists in the asymmetric unit. Both monomers in the model start from residue 9. Electron density for residues 60–72 in the dynamic loop is weak and is associated with high *B*-parameters. Statistics for data collection and refinement are shown in Table 3.

The AMP complex of Cav^- *p*FBPase is in the T-state, with a 15° subunit pair rotation and a disengaged loop 50–72. One molecule each of Fru-6-P, Mg^{2+}, P_i, and AMP binds to each subunit. The root mean square deviation in Cα carbons between AMP complexes of Cav^- and wild-type *p*FBPase (both in the T-state) is 0.3 Å. Further details regarding the structure of the AMP complex of *p*FBPase can be found in the literature (16).

Fru-2,6-P_2 Complex of Cav^- pFBPase (PDB Code 4GWU)—Crystals of the Fru-2,6-P_2 complex of Cav^- *p*FBPase (space group *I222*, a = 54.00 Å, b = 81.22 Å, and c = 165.06 Å) belong to the same space group and lattice as crystals of wild-type *p*FBPase in its R-state (PDB code 1CNQ). The asymmetric unit is a monomer. Electron density for residues 1–9 and 52–70 is absent. Electron density for residues 22–27 at the AMP binding site is weak, consistent with the previously reported R-state structure (49). Side chains of His^{45} and Tyr^{186} are clear in electron density maps, whereas the side chain of Arg^{46} is partially disordered (Fig. 3). Electron density confirms the presence of bound Fru-2,6-P_2. Mg^{2+} at metal site-1 is in contact with the 1-hydroxyl group and 2-phosphoryl group of Fru-2,6-P_2.

Superposition of the entire tetramer of the Fru-2,6-P_2 complex of Cav^- *p*FBPase onto the wild-type R-state, wild-type Fru-2,6-P_2 complex, and wild-type T-state yields root mean square deviations in C_α coordinates of 0.75, 2.3, and 2.5 Å, respectively. The Fru-2,6-P_2 complex of Cav^- *p*FBPase is near the canonical R-state, exhibiting a 2° subunit pair rotation as opposed to the 13° rotation of the Fru-2,6-P_2 complex of wild-type *p*FBPase (14) (Fig. 3). The 2° rotation in Fru-2,6-P_2 complex of Cav^- *p*FBPase is similar to the 3° rotation of the I_R-state induced by AMP in Leu^{54} *p*FBPase (23). The shearing of helices H1 and H2 observed in the AMP complex of Leu^{54} *p*FBPase is evident in the Fru-2,6-P_2 complex of Cav^- *p*FBPase, as is the loss of the hydrogen bond between Asn^{35} and Thr^{14} and the movement of Ile^{10} from its hydrophobic pocket (Fig. 3); however, unlike the AMP complex of Leu^{54} FBPase, disruption of the Glu^{192}-Thr^{39} hydrogen bond across the C1-C4 subunit interface does not occur.

TABLE 3
Statistics of data collection and refinement for Cav^- FBPase

	Fru-2,6-P_2 complex	AMP complex
Space group	I222	$P2_12_12$
Unit cell lengths (Å)	54.00, 81.22, 165.06	60.24, 164.29, 79.14
Unit cell angles (degrees)	90, 90, 90	90, 90, 90
Resolution limit (Å)	3.00	2.75
No. of measurements	26,045	50,125
No. of unique reflections	7478	17,334
Completeness of data (%)		
Overall	98.4	82.0
Last shell/resolution range (Å)	99.9/3.11–3.00	85.5/2.85–2.75
R_{sym}[a]		
Overall	0.163	0.100
Last shell/resolution range (Å)	0.516/3.11–3.00	0.272/2.85–2.75
No. of reflections in refinement	7104	16,412
Number of atoms	2489	5399
Number of solvent sites	88	281
R_{factor}[b]	0.229	0.203
R_{free}[c]	0.284	0.262
Mean B (Å^2) overall/protein	54/54	22/22
Mean B (Å^2) for Fru-2,6-P_2	47	
Mean B (Å^2) for AMP		29
Root mean square deviations		
Bond lengths (Å)	0.026	0.023
Bond angles (degrees)	1.8	1.8
Ramachandran statistics		
Preferred (%)	98.6	98.7
Outlier (%)	0	0

[a] $R_{sym} = \Sigma_i\Sigma_j|I_{ij} - \langle I_j\rangle|/\Sigma_i\Sigma_j I_{ij}$, where i runs over multiple observations of the same intensity, and j runs over all crystallographically unique intensities.
[b] $R_{factor} = \Sigma\ ||F_{obs}| - |F_{calc}||/\Sigma|F_{obs}|$, where $|F_{obs}| > 0$.
[c] R_{free} based upon 10% of the data randomly culled and not used in the refinement.

Fru-2,6-P_2 induces local conformational change in Cav^- *p*FBPase similar to that induced in wild-type *p*FBPase (Fig. 3) (14). Loop 121–126 moves toward Fru-2,6-P_2 probably in response to hydrogen bonds formed between backbone amide groups of Ser^{123} and Ser^{124} and the 2-phosphoryl group of Fru-2,6-P_2. α-Carbons of Glu^{97} and Glu^{98} move toward the Mg^{2+} at site-1, most likely a consequence of altered metal coordination due to the absence of metal at site-2. Movements in residues 97–98 and 121–126 may block Asp^{74} from forming a functionally essential hydrogen bond with the C-terminal end of loop 50–72. Loop 50–72 itself is disordered, and metal cations are absent from sites 2 and 3. The conformation of loop 264–274 in the Fru-2,6-P_2 complex of Cav^- *p*FBPase is nearly identical to that of the product complex of wild-type *p*FBPase (R-state), having not undergone the conformational change observed in the R- to T-state transition.

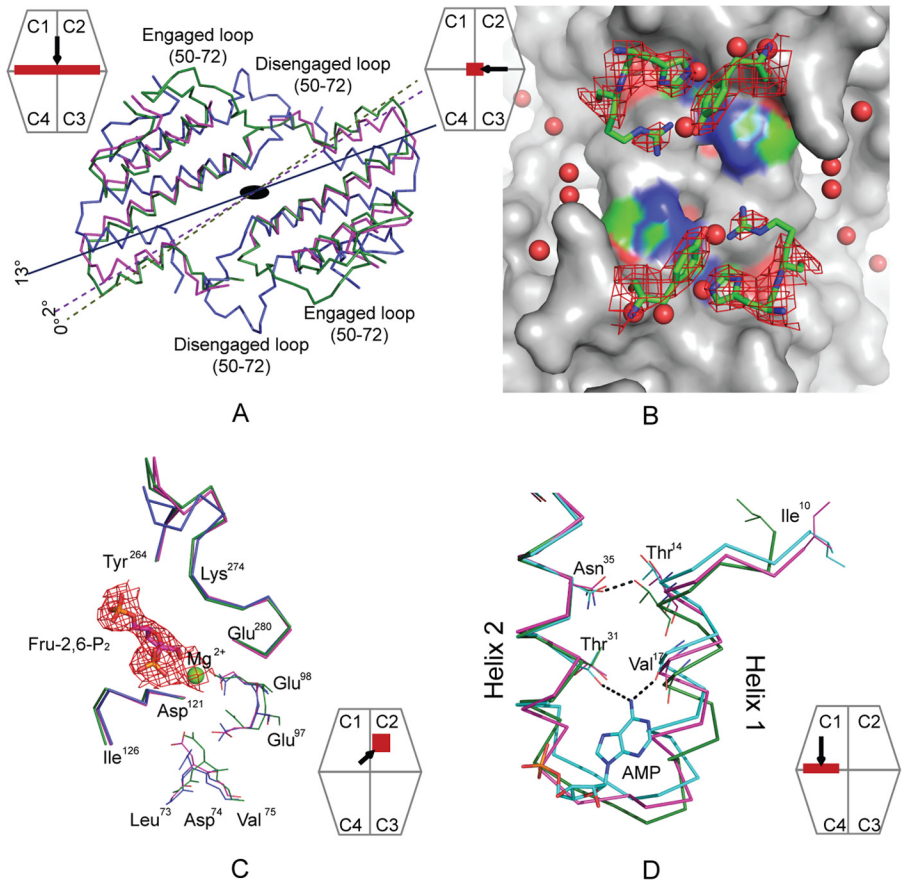

FIGURE 3. **Conformational changes of Cav$^-$ *p*FBPase induced by Fru-2,6-P_2.** *A*, subunit pair rotations induced by Fru-2,6-P_2 in wild-type (*blue*, 13°, PDB code 2QVV) and Cav$^-$ *p*FBPase (*magenta*, 2°) relative to R-state *p*FBPase (*green*, PDB code 1CNQ). C1–C2 subunit pairs are aligned, and residues 10–100 in C3–C4 subunit pairs are drawn as Cα traces. *B*, central cavity in Fru-2,6-P_2 complexes of Cav$^-$ *p*FBPase, showing electron density (contour level, 1σ) for mutated residues His^{45}, Arg^{46}, and Tyr^{186}. The image was generated with PyMOL (57). *C*, conformational differences at the active site for the Fru-2,6-P_2 complex of Cav$^-$ *p*PBPase (*magenta*), the product complex of wild-type *p*FBPase (*green*; PDB code 1CNQ), and the Fru-2,6-P_2 complex of wild-type *p*FBPase (*blue*). Individual subunits are aligned to eliminate differences due to subunit pair rotations. Electron density (contour level, 1σ) is provided for Fru-2,6-P_2 and Mg^{2+}. *D*, conformational differences at the AMP site for the Fru-2,6-P_2 complex of Cav$^-$ *p*FBPase (*magenta*), the AMP complex of Leu^{54} *p*FBPase (*cyan*; PDB code 1YYZ), and the R-state product complex of wild-type *p*FBPase (*green*; PDB code 1CNQ). *Dotted lines* indicate hydrogen bonds. The relative positions of helices H1 and H2 are similar in the Fru-2,6-P_2 complex of Cav$^-$ *p*FBPase and AMP complex of Leu^{54} *p*FBPase, which have subunit pair rotations of 2 and 3°, respectively, relative to the R-state product complex of wild-type *p*FBPase. *Icons* represent the region viewed and viewing direction.

Sequence Analysis of Type I FBPases—The alignment and hierarchical clustering of 307 Type I FBPase sequences from the Uniprot database (50) employed the ClustalW Web server on the GenomeNet database. Comparisons of sequence positions occupied by signature residues responsible for AMP inhibition, tetramer stability, Glc-6-P inhibition, phosphoenolpyruvate activation, and cavity formation segregate FBPases into groups with mutually exclusive regulatory mechanisms. Position 45, for instance, is a small side-chain residue in eukaryotic FBPases but large and hydrophilic in *E. coli*-like FBPases (Fig. 4). Residue 112 is critical for AMP inhibition (42) and is lysine in the vast majority of eukaryotic and *E. coli*-like FBPases. The salt link between Lys^{42} and Glu^{192} is essential to tetramer stability, and position 192 is glutamate in eukaryotic FBPase but a non-charged residue type in *E. coli*-like FBPases (30, 31). Positive charges at positions 228 and 38 are important for Glu-6-P inhibition and anion activation in *e*FBPase, respectively, both of which are absent in eukaryotic FBPases (30–32).

The association of residue type with regulatory mechanism facilitates the prediction of regulatory properties of FBPases that have yet to be studied experimentally. Sequences of eukaryotic FBPases fall into blocks of relatively high similarity corresponding to fungi, mammalian muscle, mammalian liver, and plants (Fig. 5). The eukaryotic FBPases should be stable tetramers subject to synergistic inhibition by AMP and Fru-2,6-P_2 (signature residues are present for the AMP site, tetramer stability, and central cavity). A block with 64 sequences in the middle of the similarity matrix includes *e*FBPase. *E. coli*-like FBPases have residue types associated with phosphoenolpyruvate activation, a dynamic equilibrium between dimer and tetramer forms, AMP inhibition, no central cavity, and, hence, no AMP/Fru-2,6-P_2 synergism. More than half of all similarity blocks have scant or no experimental data. FBPases in the large block at the top right of the similarity matrix, for instance, should lack all known mechanisms of FBPase inhibition (AMP and/or Glc-6-P inhibition or reversible disulfide bond formation) and yet be stable tetramers.

Kinetics of lFBPase—FBPases from *Leptospira* are between eukaryotic and *E. coli*-like FBPases in the similarity matrix but resemble eukaryotic FBPases, having signature residues for AMP inhibition, tetramer formation, and AMP/Fru-2,6-P_2 synergism. A bacterial FBPase with properties of a eukaryotic

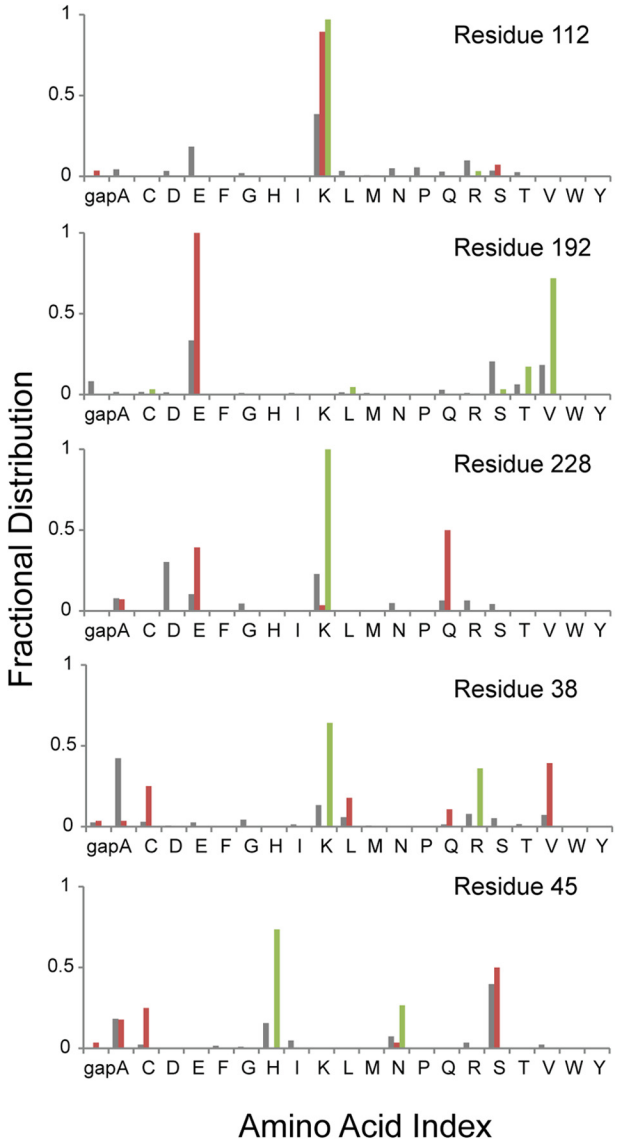

FIGURE 4. **Conservation of signature residues associated with regulatory mechanisms of FBPase.** Amino acid types associated with sequence positions essential for AMP inhibition (residue 112), tetramer formation (residue 192), Glc-6-P inhibition (residue 228), anion activation (residue 38), and central cavity formation (residue 45) are presented from *top* to *bottom*. *Gray*, *red*, and *green columns* represent the amino acid type for all FBPases, eukaryotic FBPases, and *E. coli*-like FBPases, respectively.

FBPase would suggest a pathway for the evolution of regulatory mechanisms, but the predicted properties of *l*FBPase first need confirmation by direct measurement.

Potassium activates *p*FBPase at millimolar concentrations (1, 2, 51) but inhibits *l*FBPase. Hence, assays here for *l*FBPase omit KCl. *l*FBPase catalyzes the hydrolysis of Fru-1,6-P_2 with specific activity and K_m values comparable with those of *p*FBPase. Mg^{2+} is an essential cofactor, but unlike *p*FBPase, Mg^{2+} activation is not cooperative in *l*FBPase catalysis (Table 1). Loss of Mg^{2+} cooperativity may be due to the change in residue type (aspartate to glutamate) at position 68 (*p*FBPase numerology). The mutation $Asp^{68} \rightarrow Glu$ in *p*FBPase reduces Mg^{2+} cooperativity (46), and *e*FBPase has glutamate at position 68 with no Mg^{2+} cooperativity (52). All other Mg^{2+}-binding residues are identical among the three wild-type FBPases under consideration here.

AMP inhibition of *l*FBPase is comparable with that of *p*FBPase. The Hill coefficient for AMP inhibition is close to 2. AMP is a competitive inhibitor with respect to Mg^{2+} (K_i = 0.58 ± 0.05 μM) and a non-competitive inhibitor with respect to Fru-1,6-P_2 ($K_i = K_{is}$ = 0.83 ± 0.05 μM).

Although the genome does not reveal an obvious candidate for a fructose-6-phosphate-2-kinase in *L. interrogans*, Fru-2,6-P_2 is a potent inhibitor of *l*FBPase (Table 1), competitive with substrate. In the presence of saturating substrate (20 μM) and Mg^{2+} (5 mM), the concentration of Fru-2,6-P_2 causing 50% inhibition is 0.33 ± 0.02 μM, with a Hill coefficient 1.05 ± 0.08.

Fru-2,6-P_2 enhances AMP inhibition of *l*FBPase by 15-fold (Table 2), confirming the prediction from sequence analysis. The Hill coefficient for AMP inhibition drops from 2.2 to unity upon the addition of Fru-2,6-P_2. AMP at a concentration that causes 50% inhibition (1.8 μM) enhances Fru-2,6-P_2 inhibition by 2-fold (Fig. 6).

Anion activators, such as PEP or citrate, activate *e*FBPase by promoting tetramer formation (31). To test the effect of PEP on *l*FBPase, Mg^{2+}-initialized assays were used (31). PEP activation is not present for *l*FBPase. Instead, millimolar levels of PEP cause moderate inhibition. Assays of Glc-6-P inhibition followed the published protocol for *e*FBPase (32). Glc-6-P inhibition becomes evident only at millimolar levels, ~50-fold weaker than Glc-6-P inhibition of *e*FBPase. Glc-6-P inhibits *p*FBPase and *l*FBPase at comparable concentrations.

Sedimentation Equilibrium—*l*FBPase and *p*FBPase at three protein concentrations (A_{280} = 0.3, 0.5, and 0.7) were sedimented to equilibrium at angular speeds of 15,000, 18,000 and 21,000 rpm. Sedimentation equilibrium data were fit to single component and dimer-tetramer equilibrium models with UltraScan (53). Regardless of model, *p*FBPase and *l*FBPase give similar apparent molecular masses, 111.9 and 112.1 kDa, respectively. The determined molecular masses are less than the calculated mass of the tetramer (140 kDa).

Tryptophan Fluorescence—*l*FBPase has but one tryptophan (Trp^{219}), which on the basis of structural similarity is near the common binding sites for the 6-phosphoryl groups of substrate, product, and Fru-2,6-P_2. Steady-state fluorescence emission from Trp^{219} increases as levels of substrate, product, or Fru-2,6-P_2 increase, whereas increasing concentrations of AMP cause little change. Substrate, product, Fru-2,6-P_2, and AMP have no effect on fluorescence emission from 100 μM tryptophan in the absence of *l*FBPase. The fluorescence change caused by Fru-6-P, Fru-1,6-P_2, or Fru-2,6-P_2 is arguably due to a change in the local environment of Trp^{219}. Indeed, at saturating concentrations, the three active site ligands induce nearly identical limiting changes in fluorescence emission.

Data from titrations of 6-phosphoryl ligands in the presence and absence of AMP are fit to Equation 3,

$$\frac{\Delta F}{F_0} = \left(\frac{\Delta F_{max}}{F_0}\right) \cdot \frac{L}{K_d + L} \qquad \text{(Eq. 3)}$$

where ΔF is the change in fluorescence upon the addition of ligand L, F_o is the fluorescence in the absence of ligand, and K_d is the dissociation constant. AMP does not affect the binding of Fru-1,6-P_2 (Fig. 6 and Table 4); however, AMP at a concentra-

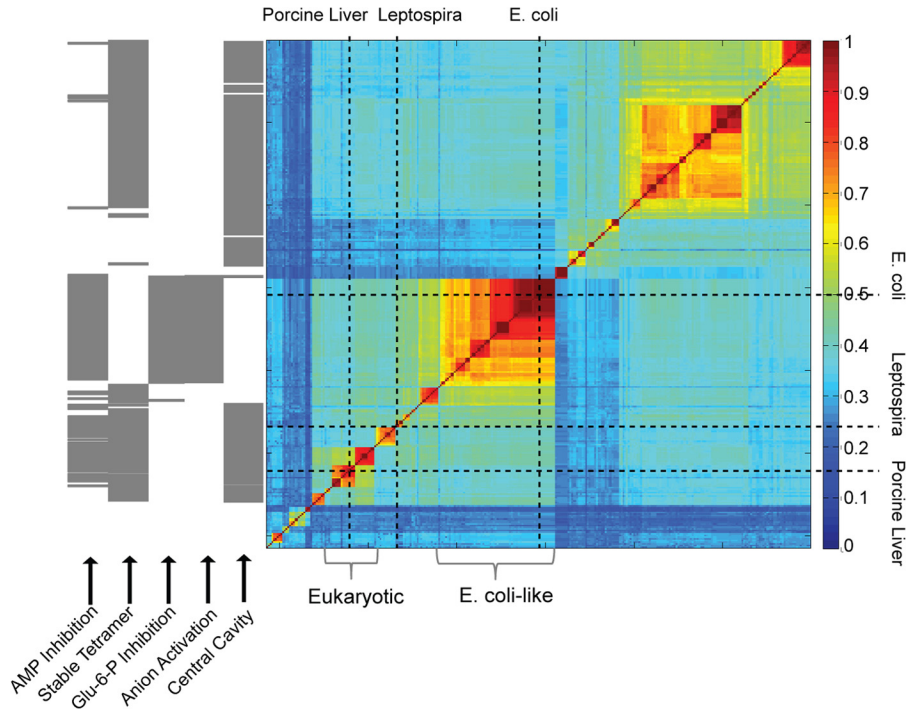

FIGURE 5. **Similarity matrix of Type I FBPase sequences and the prediction of structural and regulatory properties.** The fraction of identical residues in sequence pairs are represented by *color* according to the *scale* to the *right* of the similarity matrix. The positions of *e*FBPase, *p*FBPase, and *l*FBPase are marked by *vertical* and *horizontal dotted lines*. FBPases from eukaryotic systems and *E. coli*-like FBPases are indicated by *brackets*. Regulatory properties are predicted (*gray bar*) according to residue types associated with key positions in the amino acid sequence. AMP inhibition requires serine or threonine for residue 31, lysine or arginine for residue 112, and tyrosine for residue 113. Tetramer stability requires lysine or arginine for residue 42 and glutamate for residue 192. Glc-6-P inhibition requires tyrosine for residue 216, lysine or arginine for residue 228, and glutamine for residue 231. Anion activation requires glycine for residue 14, lysine or arginine for residue 38, lysine or arginine for residue 88, and not glutamate for residue 192. The presence of a central cavity (AMP/Fru-2,6-P_2 synergism) requires small side chains (glycine, alanine, cysteine, serine, or gap) for residue 45.

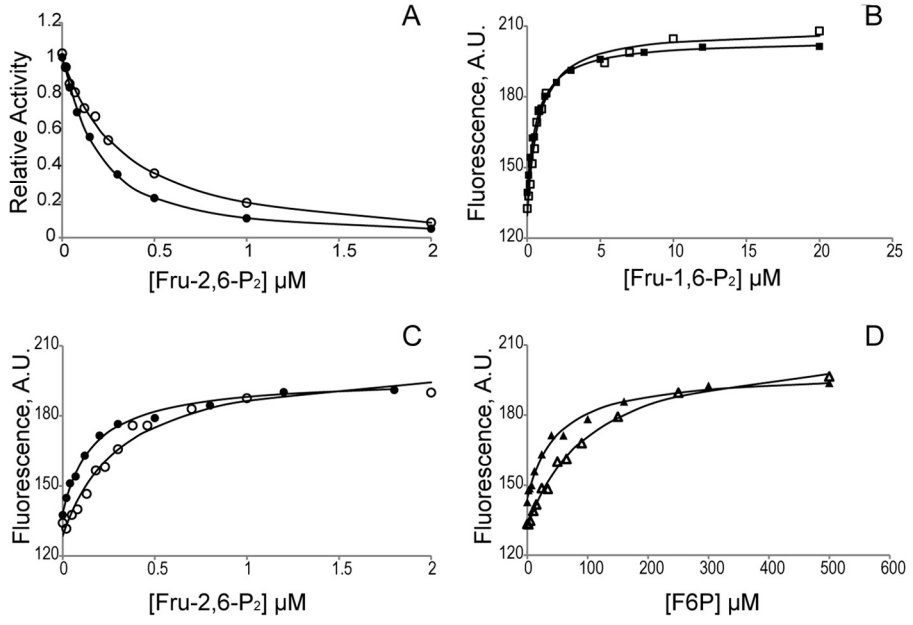

FIGURE 6. **Synergism between active site ligands and AMP in *l*FBPase.** *A*, Fru-2,6-P_2 inhibition in the absence (○) and presence (●) of AMP ([AMP] = $I_{0.5}$-AMP = 1.8 μM). All assays are carried out with saturating Fru-1,6-P_2 (20 μM) and Mg^{2+} (10 mM). *B–D*, titrations for Fru-1,6-P_2 (*B*), Fru-2,6-P_2 (*C*), and Fru-6-P (*D*) performed in the absence (*open symbols*) and presence (*filled symbols*) of AMP ([AMP] = $I_{0.5}$-AMP = 1.8 μM) reveal binding synergism between AMP and only Fru-6-P and Fru-2,6-P_2. Each titration data point represents integration of the Trp^{219} emission spectrum from 310 to 370 nm.

tion that causes 50% inhibition (1.8 μM) enhances the binding of Fru-2,6-P_2 by ~2-fold, consistent with data from kinetics. AMP enhancement of Fru-6-P binding to *l*FBPase is also 2-fold, suggesting that the reverse effect (Fru-6-P enhancement of AMP binding) is comparable with Fru-2,6-P_2 enhancement (15-fold; Table 2). Fru-6-P enhancement of AMP binding cannot be measured because of assay design (coupling of Fru-6-P production to NADPH formation).

TABLE 4
Effect of AMP on the binding of ligands to the active site
S.D. in the last significant digit is given parenthetically.

Ligand	K_d ([AMP] = 0)	K_d ([AMP] = 1.8 μM)
	μM	μM
Fru-1,6-P_2	0.77 (9)	0.73 (5)
Fru-2,6-P_2	0.32 (7)	0.17 (2)
Fru-6-P	105 (9)	50 (7)

DISCUSSION

Ser^{45} → His and Cav^- *p*FBPases represent first instances of modified *p*FBPases that retain potent AMP and Fru-2,6-P_2 inhibition with greatly reduced AMP/Fru-2,6-P_2 synergism. Kinetic parameters for catalysis, Mg^{2+} activation, AMP inhibition, and Fru-2,6-P_2 inhibition of mutant enzymes investigated here are similar to those of wild-type *p*FBPase. Reduced Fru-2,6-P_2/AMP synergism in Cav^- *p*FBPase is not due to the disruption of the active or allosteric binding sites but rather to an impaired quaternary response; Cav^- *p*FBPase exhibits only a 2° subunit pair rotation in contrast to the 13° subunit pair rotation for the wild-type enzyme. Conceivably, Cav^- mutations could stabilize the R-state (or destabilize the T-state), making the quaternary transition unfavorable; however, previously reported mutations that destabilize quaternary states (Ala^{54} → Leu and Ile^{10} → Asp, for instance) broadly impact the kinetics of *p*FBPase. Moreover, impairment of the R- to T-state transition is specific to Fru-2,6-P_2. AMP drives Cav^- *p*FBPase to a canonical T-state, which is structurally indistinguishable from the T-state of the wild-type enzyme.

The effect of Fru-2,6-P_2 must be more than the displacement of loop 50–72 from its engaged conformation. Loop 50–72 is disordered in the Fru-2,6-P_2 complex of Cav^- *p*FBPase, but the enzyme remains in an R-like state. In contrast, the loop 50–72 acquires its disengaged conformation in the Fru-2,6-P_2 complex of wild-type *p*FBPase, and the enzyme is in a near-T quaternary state. Structural evidence here indicates the subunit pair rotation must go beyond 2° to allow the disengaged conformer.

The solvated central cavity, absent in Cav^- *p*FBPase, evidently enables the requisite subunit pair rotation in response to the binding of Fru-2,6-P_2. The binding of AMP to Leu^{54} *p*FBPase causes a 3° subunit pair rotation, retaining the engaged conformation of loop 50–72 (23) and an organized water structure in the central cavity (Fig. 1). In contrast, in the T-state of Leu^{54} *p*FBPase, loop 50–72 and the water structure in the cavity are disordered. Arguably, an order-to-disorder transition of water molecules within the central cavity, caused by the movement of loop 50–72 from its engaged conformation, provides the requisite motive force for subunit pair rotation. In Cav^- *p*FBPase, the order-to-disorder transition of water structure is inoperative, and consequently movement of loop 50–72 from its engaged conformation results in virtually no subunit pair rotation. The mutation of Ser^{45} → His alone is largely responsible for this effect, suggesting a critical role for Ser^{45} in maintaining an organized water structure when loop 50–72 is engaged. The volume of the histidyl side chain (137 $Å^3$) relative to that of serine (89 $Å^3$) is probably a factor; however, the side chain of serine in this specific context may offer the capacity, not shared by other amino acid types, to "seed" a network of hydrogen-bonded water molecules.

Fru-2,6-P_2/AMP synergism, although reduced, is still present in His^{45} and Cav^- *p*FBPase. The 2° subunit pair rotation caused by Fru-2,6-P_2 in Cav^- *p*FBPase is similar to changes induced by AMP in Leu^{54} *p*FBPase (I_R-state, 3° subunit pair rotation). Structural changes at the C1-C4 interface due to small subunit pair rotations could be the structural basis for the weak synergism that remains in Cav^- *p*FBPase. Indeed, wild-type and mutant *p*FBPases here exhibit reduced AMP cooperativity in the presence of Fru-2,6-P_2, which may come from conformational changes at the C1-C4 interface (such as the weakening of the hydrogen bond between Glu^{192} and Thr^{39}) within the first few degrees of subunit pair rotation. The model above suggests that an engaged dynamic loop in the presence of bound Fru-2,6-P_2 would eliminate Fru-2,6-P_2/AMP synergism altogether, and in fact, such is the case for *e*FBPase; there is no Fru-2,6-P_2/AMP synergism, and the Fru-2,6-P_2 complex of wild-type *e*FBPase reveals a dynamic loop in its engaged conformation (14).

The failure of the loop 50–72 to achieve a disengaged conformation in its Fru-2,6-P_2 complex of Cav^- *p*FBPase is also consistent with the results of targeted molecular dynamics simulations, which indicate that the transition of loop 50–72 from an engaged to disengaged conformation comes late in the R- to T-state transition (24). Moreover, previous work ties the conformational change in loop 264–274 to subunit pair rotation from the I_R- to I_T-state (from 3 to 12°, respectively) (23, 24). The Fru-2,6-P_2 complexes of Cav^- and wild-type *p*FBPases reveal a conformational change in loop 264–274 only for the latter complex.

The foregoing analysis supports the following hypothesis. Any tetrameric FBPase with signature residues of a central cavity should exhibit AMP/Fru-2,6-P_2 synergism. Hence, all eukaryotic organisms for which sequences of FBPases are known should exhibit AMP/Fru-2,6-P_2 synergism.

Fru-2,6-P_2 is not present in bacteria (54), so the evolution of AMP/Fru-2,6-P_2 synergism from a bacterial ancestor is problematic. *E. coli* FBPase employs Glc-6-P as a synergistic inhibitor with respect to AMP (32). Unlike Fru-2,6-P_2, Glc-6-P is an allosteric non-competitive inhibitor with respect to substrate. Vastly different kinetic properties and a distinct allosteric binding site for Glc-6-P in *e*FBPase make Glc-6-P an unlikely precursor of Fru-2,6-P_2 through evolution. The analysis of Type I FBPase sequences, however, indicates a central cavity in *l*FBPase. Moreover, AMP/Fru-6-P binding synergism in *l*FBPase suggests an evolutionary pathway from AMP/Fru-6-P synergism in bacteria to AMP/Fru-2,6-P_2 synergism in eukaryotic organisms.

At some point in evolution, a primordial FBPase may have existed as an equilibrium mixture of dimers and tetramers (Fig. 7). This primordial FBPase may have been subject to AMP inhibition and feedback inhibition by Fru-6-P. One pathway of evolution stabilizes the tetramer through the creation of an anion activation site. Over time, this form of FBPase acquires a site for Glc-6-P inhibition that acts synergistically with AMP, becoming the present day *e*FBPase.

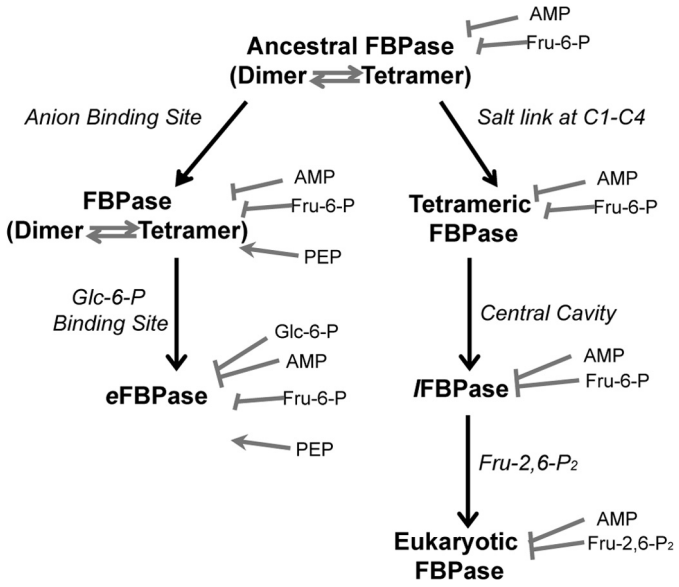

FIGURE 7. **Proposed evolution of the regulatory properties of FBPases.** Different pathways to a stable tetramer (anion binding site *versus* salt link formation) led to *E. coli*-like and eukaryotic mechanisms of regulation.

An alternative pathway of evolution also leads to a stable FBPase tetramer through the formation of Glu^{192}–Lys^{42} salt links. Because this form of the tetramer is at all times catalytically competent, a robust mechanism of inhibition would presumably co-evolve. Mutation of position 45 from histidine to serine would create a nascent central cavity in the primordial enzyme with no effect on activity. The introduction of the Glu^{192}–Lys^{42} salt link in a Ser^{45} ancestral FBPase would create a stable tetramer with a central cavity. The central cavity would enable AMP/Fru-6-P synergism as a counterpoint to the enhanced activity of a stable tetramer. Over time, Fru-2,6-P_2 replaces Fru-6-P as a dynamic regulator. Crystal structures of Fru-2,6-P_2 bound to *p*FBPase clearly show that all atoms, excepting the 2-phosphoryl group, occupy positions corresponding to those of Fru-6-P (14).

L. interrogans is a pathogenic bacterium with a metabolism strikingly different from that of mammals (55). *L. interrogans* lacks hexokinase (as well as other enzymes of glycolysis) and cannot capture and directly use glucose from exogenous sources (55, 56). Instead, lipid is the principal energy source for *L. interrogans*.

The apparent role of gluconeogenesis in *L. interrogans* is the generation of Fru-6-P as a precursor for sugar-nucleotide biosynthesis (56). Given that a gene coding for glucose 6-phosphate dehydrogenase is absent in *L. interrogans* (56), Fru-6-P must enter the non-oxidative pentose phosphate pathway in order to produce ribose 5-phosphate. The conversion of Fru-1,6-P_2 into Fru-6-P in *L. interrogans* then represents the first committed step in ribose 5-phosphate biosynthesis and *de novo* nucleotide biosynthesis. In this scheme, Fru-6-P is a direct feedback inhibitor, and AMP is an allosteric feedback inhibitor. High levels of Fru-6-P should affect only *l*FBPase, due to the absence of a glycolytic pathway. When nucleotides are in demand, the concentrations of AMP and Fru-6-P (the latter being in equilibrium with the pool of ribose 5-phosphate) should be low; however, rising concentrations of AMP and Fru-6-P may synergistically support each other in the feedback inhibition of *l*FBPase.

Leptospira is the causative agent of leptospirosis, a disease of global concern, causing renal and hepatic damage and, in some instances, sudden and fatal hemoptysis (55). Infections in livestock and domestic animals can expose humans to *Leptospira* infections through sanitary waste or contaminated drinking water. Little information is known about the metabolism of *L. interrogans* by direct experimentation. Given the current status of our knowledge, however, one could regard FBPase from *Leptospira* as a potential target in the development of agents of anti-microbial growth.

REFERENCES

1. Benkovic, S. J., and deMaine, M. M. (1982) Mechanism of action of fructose 1,6-bisphosphatase. *Adv. Enzymol. Relat. Areas Mol. Biol.* **53,** 45–82
2. Tejwani, G. A. (1983) Regulation of fructose-bisphosphatase activity. *Adv. Enzymol. Relat. Areas Mol. Biol.* **54,** 121–194
3. Blangy, D., Buc, H., and Monod, J. (1968) Kinetics of the allosteric interactions of phosphofructokinase from *Escherichia coli*. *J. Mol. Biol.* **31,** 13–35
4. Taketa, K., and Pogell, B. M. (1965) Allosteric inhibition of rat liver fructose 1,6-bisphosphatase by adenosine 5′-monophosphate. *J. Biol. Chem.* **240,** 651–662
5. Pilkis, S. J., El-Maghrabi, M. R., Pilkis, J., and Claus, T. (1981) Inhibition of fructose-1,6-bisphosphatase by fructose 2,6-bisphosphate. *J. Biol. Chem.* **256,** 3619–3622
6. Van Schaftingen, E., and Hers, H.-G. (1981) Inhibition of fructose-1,6-bisphosphatase by fructose 2,6-biphosphate. *Proc. Natl. Acad. Sci. U.S.A.* **78,** 2861–2863
7. Pilkis S. J., El-Maghrabi, M. R., Pilkis, J., Claus, T. H., and Cumming D. A. (1981) Fructose 2,6-bisphosphate. A new activator of phosphofructokinase. *J. Biol. Chem.* **256,** 3171–3174
8. Van Schaftingen, E., Jett, M.-F., Hue, L., and Hers, H.-G. (1981) Control of liver 6-phosphofructokinase by fructose 2,6-bisphosphate and other effectors. *Proc. Natl. Acad. Sci. U.S.A.* **78,** 3483–3486
9. Uyeda, K., Furuya, E., and Luby, L. J. (1981) The effect of natural and synthetic D-fructose 2,6-bisphosphate on the regulatory kinetic properties of liver and muscle phosphofructokinase. *J. Biol. Chem.* **256,** 8394–8399
10. Okar, D. A., and Lange, A. J. (1999) Fructose-2,6-bisphosphate and control of carbohydrate metabolism in eukaryotes. *Biofactors* **10,** 1–14
11. Derr, R. F., and Zieve, L. (1972) Adenylate energy charge. Relation to guanylate energy charge and the adenylate kinase equilibrium constant. *Biochem. Biophys. Res. Commun.* **49,** 1385–1390
12. Han, P. F., Han, G. Y., Hayes, R. L., Moore, C. L., and Johnson, J. (1983) Synergistic effect of AMP and fructose 2,6-bisphosphate on the protection of fructose 1,6-bisphosphatase against inactivation by trypsin. *Experientia* **39,** 1305–1307
13. Kruger, N. J., and Beevers, H. (1984) Effect of fructose 2,6-bisphosphate on the kinetic properties of cytoplasmic fructose 1,6-bisphosphatase from germinating castor bean endosperm. *Plant Physiol.* **76,** 49–54
14. Hines, J. K., Chen, X., Nix, J. C., Fromm, H. J., and Honzatko, R. B. (2007) Structures of mammalian and bacterial fructose-1,6-bisphosphatase reveal the basis for synergism in AMP/fructose 2,6-bisphosphate inhibition. *J. Biol. Chem.* **282,** 36121–36131
15. Ke, H. M., Zhang, Y. P., and Lipscomb, W. N. (1990) Crystal structure of fructose-1,6-bisphosphatase complexed with fructose 6-phosphate, AMP and magnesium. *Proc. Natl. Acad. Sci. U.S.A.* **87,** 5243–5247
16. Choe, J. Y., Fromm, H. J., and Honzatko, R. B. (2000) Crystal structures of fructose 1,6-bisphosphatase. Mechanism of catalysis and allosteric inhibition revealed in product complexes. *Biochemistry* **39,** 8565–8574
17. Scheffler, J. E., and Fromm, H. J. (1986) Regulation of rabbit liver fructose-1,6-bisphosphatase by metals, nucleotides, and fructose 2,6-bisphosphate as determined from fluorescence studies. *Biochemistry* **25,** 6659–6665
18. Liu, F., and Fromm, H. J. (1988) Purification and characterization of fructose-1,6-bisphosphatase from bovine brain. *Arch. Biochem. Biophys.* **260,**

609–615
19. Zhang, Y., Liang, J. Y., Huang, S., and Lipscomb, W. N. (1994) Toward a mechanism for the allosteric transition of pig kidney fructose-1,6-bisphosphatase. *J. Mol. Biol.* **244,** 609–624
20. Nelson, S. W., Honzatko, R. B., and Fromm, H. J. (2002) Hybrid tetramers of porcine liver fructose-1,6-bisphosphatase reveal multiple pathways of allosteric inhibition. *J. Biol. Chem.* **277,** 15539–15545
21. Shyur, L.-F., Aleshin, A. E., Honzatko, R. B., and Fromm, H. J. (1996) Site-directed mutagenesis of residues at subunit interfaces of porcine fructose-1,6-bisphosphatase. *J. Biol. Chem.* **271,** 3005–3010
22. Shyur, L.-F., Aleshin, A. E., Honzatko, R. B., and Fromm, H. J. (1996) Biochemical properties of mutant and wild-type fructose-1,6-bisphosphatases are consistent with the coupling of intra- and intersubunit conformational changes in the T- and R-state transition. *J. Biol. Chem.* **271,** 33301–33307
23. Iancu, C. V., Mukund, S., Fromm, H. J., and Honzatko, R. B. (2005) R-state AMP complex reveals initial steps of the quaternary transition of fructose-1,6-bisphosphatase. *J. Biol. Chem.* **280,** 19737–19745
24. Gao, Y., Iancu, C. V., Mukind, S., Choe, J. Y., and Honzatko, R. B. (2013) Mechanism of displacement of catalytically essential loop from the active site of mammalian fructose-1,6-bisphosphatase. *Biochemistry* **52,** 5206–5216
25. Ganson, N. J., and Fromm, H. J. (1985) Nuclear magnetic resonance studies of fructose 2,6-bisphosphate and adenosine 5′-monophosphate interaction with bovine liver fructose-1,6-bisphosphatase. *J. Biol. Chem.* **260,** 2837–2843
26. Liu, F., and Fromm, H. J. (1988) Interaction of fructose 2,6-bisphosphate and AMP with fructose-1,6-bisphosphatase as studied by nuclear magnetic resonance spectroscopy. *J. Biol. Chem.* **263,** 9122–9128
27. Liu, F., and Fromm, H. J. (1988) Relationship between thiol group modification and the binding site for fructose 2,6-bisphosphate on rat liver fructose-1,6-bisphosphatase. *J. Biol. Chem.* **263,** 10035–10039
28. Xue, Y., Huang, S., Liang, J.-Y., and Lipscomb, W. N. (1994) Crystal structure of fructose-1,6-bisphosphatase complexed with fructose 2,6-bisphosphate, AMP and Zn^{2+} at 2.0-Å resolution. Aspects of synergism between inhibitors. *Proc. Natl. Acad. Sci. U.S.A.* **91,** 12482–12486
29. McGrane, M. M., El-Maghrabi, M. R., and Pilkis, S. J. (1983) The interaction of fructose 2,6-bisphosphate and AMP with rat hepatic fructose 1,6-bisphosphatase. *J. Biol. Chem.* **258,** 10445–10454
30. Hines, J. K., Fromm, H. J., and Honzatko, R. B. (2006) Novel allosteric activation site in *Escherichia coli* fructose-1,6-bisphosphatase. *J. Biol. Chem.* **281,** 18386–18393
31. Hines, J. K., Fromm, H. J., and Honzatko, R. B. (2007) Structures of activated fructose-1,6-bisphosphatase from *Escherichia coli*. Coordinate regulation of bacterial metabolism and the conservation of the R-state. *J. Biol. Chem.* **282,** 11696–11704
32. Hines, J. K., Kruesel, C. E., Fromm, H. J., and Honzatko, R. B. (2007) Structures of inhibited fructose-1,6-bisphosphatase from *Escherichia coli*. Distinct allosteric inhibition sites for AMP and glucose 6-phosphate and the characterization of a gluconeogenic switch. *J. Biol. Chem.* **282,** 24697–24706
33. Van Schaftingen, E., and Hers, H.-G. (1981) Formation of fructose 2,6-bisphosphate from fructose 1,6-bisphosphate by intramolecular cyclisation followed by alkaline hydrolysis. *Eur. J. Biochem.* **117,** 319–323
34. Laemmli, U. K. (1970) Cleavage of structural proteins during the assembly of the head of bacteriophage T4. *Nature* **227,** 680–685
35. Bradford, M. M. (1976) A rapid sensitive method for the quantitation of microgram quantities of protein utilizing the principle of protein-dye binding. *Anal. Biochem.* **72,** 248–254
36. Leatherbarrow, R. J. (2009) *GraFit*, version 7, Erithacus Software Ltd., Horley, UK
37. Nelson, S. W., Choe, J.-Y., Iancu, C. V., Honzatko, R. B., and Fromm, H. J. (2000) Tryptophan fluorescence reveals the conformational state of a dynamic loop in recombinant porcine fructose-1,6-bisphosphatase. *Biochemistry* **39,** 11100–11106
38. Pflugrath, J. W. (1999) The finer things in X-ray diffraction data collection. *Acta Crystallogr. D* **55,** 1718–1725
39. Brünger, A. T., Adams, P. D., Clore, G. M., DeLano, W. L., Gros, P., Grosse-Kunstleve, R. W., Jiang, J.-S., Kuszewski, J., Nilges, M., Pannu, M. S., Read, R. J., Rice, L. M., Simonson, T., Warren, G. L. (1998) Crystallography & NMR system. A new software suite for macromolecular structure determination. *Acta Crystallogr. D* **54,** 905–921
40. Engh, R. A., and Huber, R. (1991) Accurate bond and angle parameters for x-ray protein structure refinement. *Acta Crystallogr. A* **47,** 392–400
41. Chen, V. B., Arendall, W. B., 3rd, Headd, J. J., Keedy, D. A., Immormino, R. M., Kapral, G. J., Murray, L. W., Richardson, J. S., and Richardson, D. C. (2010) MolProbity. All-atom structure validation for macromolecular crystallography. *Acta Crystallogr. D* **66,** 12–21
42. Kelley-Loughnane, N., and Kantrowitz, E. R. (2001) AMP inhibition of pig kidney fructose-1,6-bisphosphatase. *Biochim. Biophys. Acta* **1548,** 66–71
43. Shyur, L. F., Poland, B. W., Honzatko, R. B., and Fromm, H. J. (1997) Major changes in the kinetic mechanism of AMP inhibition and AMP cooperativity attend the mutation of Arg49 in fructose-1,6-bisphosphatase. *J. Biol. Chem.* **272,** 26295–26299
44. Nelson, S. W., Choe, J. Y., Honzatko, R. B., and Fromm, H. J. (2000) Mutations in the hinge of a dynamic loop broadly influence functional properties of fructose-1,6-bisphosphatase. *J. Biol. Chem.* **275,** 29986–29992
45. Nelson, S. W., Kurbanov, F. T., Honzatko, R. B., and Fromm, H. J. (2001) The N-terminal segment of recombinant porcine fructose-1,6-bisphosphatase participates in the allosteric regulation of catalysis. *J. Biol. Chem.* **276,** 6119–6124
46. Kurbanov, F. T., Choe, J. Y., Honzatko, R. B., and Fromm, H. J. (1998) Directed mutations in the poorly defined region of porcine liver fructose-1,6-bisphosphatase significantly affect catalysis and the mechanism of AMP inhibition. *J. Biol. Chem.* **273,** 17511–17516
47. el-Maghrabi, M. R., Austin, L. R., Correia, J. J., and Pilkis, S. J. (1992) Lysine 274 is essential for fructose 2,6-bisphosphate inhibition of fructose-1,6-bisphosphatase. *J. Biol. Chem.* **267,** 6526–6530
48. Nelson, S. W., Honzatko, R. B., and Fromm, H. J. (2004) Origin of cooperativity in the activation of fructose-1,6-bisphosphatase by Mg^{2+}. *J. Biol. Chem.* **279,** 18481–18487
49. Choe, J. Y., Poland B. W., Fromm, H. J., and Honzatko, R. B. (1998) Role of a dynamic loop in cation activation and allosteric regulation of recombinant porcine fructose-1,6-bisphosphatase. *Biochemistry* **37,** 11441–11450
50. UniProt Consortium (2012) Reorganizing the protein space at the Universal Protein Resource (UniProt). *Nucleic Acids Res.* **40,** D71–D75
51. Zhang, R., Villeret, V., Lipscomb, W. N., and Fromm, H. J. (1996) Kinetics and mechanisms of activation and inhibition of porcine liver fructose-1,6-bisphosphatase by monovalent cations. *Biochemistry* **35,** 3038–3043
52. Kelley-Loughnane, N., Biolsi, S. A., Gibson, K. M., Lu, G., Hehir, M. J., Phelan, P., Kantrowitz, E. R. (2002) Purification, kinetic studies, and homology model of *Escherichia coli* fructose-1,6-bisphosphatase. *Biochim. Biophys. Acta* **1594,** 6–16
53. Demeler, B. (2005) UltraScan. A Comprehensive Data Analysis Software Package for Analytical Ultracentrifugation Experiments. in *Modern Analytical Ultracentrifugation: Techniques and Methods*. (Scott, D. J., Harding, S. E., and Rowe, A. J., eds) pp. 210–229, Royal Society of Chemistry, London
54. Michels, P. A., and Rigden, D. J. (2006) Evolutionary analysis of fructose 2,6-bisphosphate metabolism. *IUBMB Life* **58,** 133–141
55. Faine, S., Adler, B., Bolin, C., and Perolat, P. (1999) *Leptospira and Leptospirosis*, Medisci, Melbourne
56. Ren, S. X., Fu, G., Jiang, X. G., Zeng, R., Miao, Y. G., Xu, H., Zhang, Y. X., Xiong, H., Lu, G., Lu, L. F., Jiang, H. Q., Jia, J., Tu, Y. F., Jiang, J. X., Gu, W. Y., Zhang, Y. Q., Cai, Z., Sheng, H. H., Yin, H. F., Zhang, Y., Zhu, G. F., Wan, M., Huang, H. L., Qian, Z., Wang, S. Y., Ma, W., Yao, Z. J., Shen, Y., Qiang, B. Q., Xia, Q. C., Guo, X. K., Danchin, A., Saint Girons, I., Somerville, R. L., Wen, Y. M., Shi, M. H., Chen, Z., Xu, J. G., and Zhao, G. P. (2003) Unique physiological and pathogenic features of *Leptospira interrogans* revealed by whole-genome sequencing. *Nature* **422,** 888–893
57. DeLano, W. L. (2012) *The PyMOL Molecular Graphics System*, version 1.5.0.4 Schrödinger, LLC, New York